ISSN 1054-660X, Laser Physics, 2009, Vol. 19, No. 8, pp. 1769–1775.

Long-Distance Femtosecond Laser Filaments in Air[1]

J. Zhang[a, b], X. Lu[a], Y. Y. Ma[a, c], T. T. Xi[a, d], Y. T. Li[a], Z. M. Sheng[a, b], L. M. Chen[a], J. L. Ma[a], Q. L. Dong[a], Z. H. Wang[a], and Z. Y. Wei[a]

[a] *Laboratory of Optical Physics, Institute of Physics, Chinese Academy of Sciences, Beijing, 100190 China*
[b] *Department of Physics, Shanghai Jiao Tong University, Shanghai, 200240 China*
[c] *State Key Laboratory for Mesoscopic Physics, Department of Physics, Peking University, Beijing, 100871 China*
[d] *Department of Physics, Graduate University of Chinese Academy of Sciences, Beijing, 100049 China*
*e-mail: ytli@aphy.iphy.ac.cn
Received February 28, 2009

Abstract—This paper reviews the recent studies of filamentation of femtosecond lasers pulses in air in the Institute of Physics, Chinese Academy of Sciences. The filamentation mechanisms of free propagated femtosecond laser pulses, effect of air turbulence on the filamentation, interaction between filaments are presented.

PACS numbers: 42.65.Jx

DOI: 10.1134/S1054660X09150481

1. INTRODUCTION

The filamentation of optical laser beam in nonlinear media was observed in sixties of last century. But more than a decade ago, femtosecond (fs) pulses introduced a new concept into the "old" field. Due to the advantages of intense fs pulses, many interesting phenomena occur and potential applications, such as lightning control, remote sensing, and pulse compression attract scientists' attentions widely.

The mechanisms underlying the propagation of intense fs laser pulses have been well studied. Three models were proposed during the past decades. Braun et al. [1] proposed the self-waveguiding model to interpret the self-guided filament formation as the results of the balance between self-focusing and plasma defocusing. The main conception of self-waveguiding model can be described as follows: When high power laser pulse propagates in air, the Kerr nonlinearity can leads to self-focusing of laser pulse and the laser intensity will increase, when the laser intensity exceeds the multi-photon ionization (MPI) threshold of air, low density plasma can be generated. The plasma density gradient can induce defocusing effect to the laser propagation. The dynamic balance between the two effects leads to the self-guided propagation. Brodeur et al. [2] adopted the moving-focus model whereby different time slices of the pulse focus at different nonlinear focal lengths [3–5]. However, the moving-focus model cannot explain the persistence of a filament beyond the linear focus, and the self-waveguiding model also has some problems of interpretation [6]. The dynamic spatial replenishment model proposed by Mlejnek et al. [7] believes that the mechanism should be the periodical energy transformation between the filament and background energy reservoir. That is to say, the focusing-defocusing cycle leads to the long-distance propagation of laser pulses in air. The recurrent collapse mechanism is consistent with almost all recent experimental results.

Although the filamentation of fs laser pulses in air has been studied for many years, but many physical problems in this field are still not clearly understood and need to be investigated further. In this paper we will review our recent theoretical and numerical studies on the mechanisms' of hundreds of meters range light filaments formed by free propagated powerful fs laser pulses in atmosphere, effect of air turbulence on the filamentation, filament interaction between fs laser pulses.

2. SPATIOTEMPORAL MOVING FOCUS OF LONG FEMTOSECOND LASER FILAMENTS IN AIR

In the self-guiding and dynamic spatial replenishment models, the ionization plays an important role in the formation of filaments. In a long period, in most experiments the fs laser filamentation in air is induced with slightly focused pulses in laboratory scale [8–10]. Such kinds of filaments usually have 100–200 μm diameter, and several tens of meters length. The electron density is 10^{16}–10^{17} cm^{-3}, which can clamp the filament intensity down to 10^{14} W/cm^2 [1]. However, more and more experiments to study the hundred-meter range filamentation induced by free propagation of fs laser pulses have been performed in recent years [11–14]. The typical size of the free propagation filaments is about 1 mm, and the intensity in filament

[1] The article is published in the original.

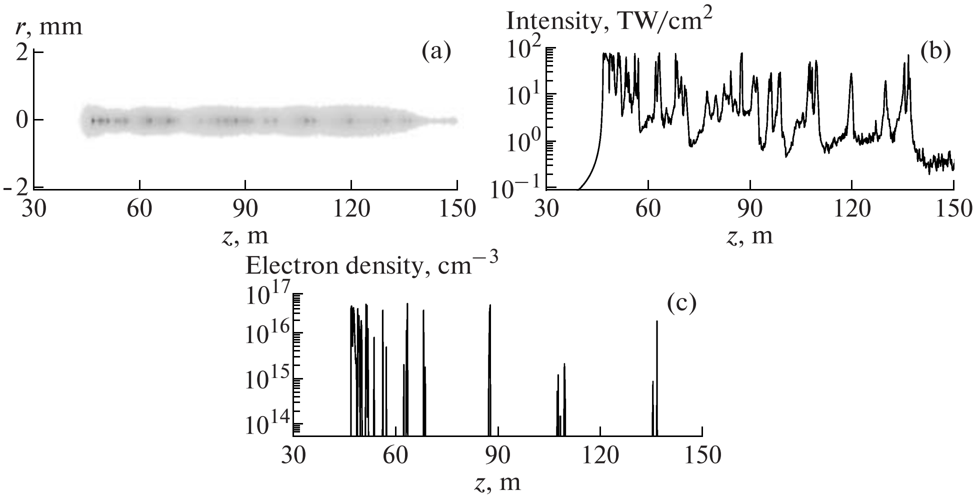

Fig. 1. Energy fluence distribution (a), peak intensity (b), and peak electron density of the fs laser filament as a function of propagation distance z (c).

is just above the ionization threshold. The ionization at such intensity can be estimated using multiphoton ionization model. The electron density is only about 10^{13} cm^{-3} [12]. The refraction index change by such low electron density is several orders lower than that caused by Kerr nonlinearity. In this case, the ionization defocusing can not balance the Kerr self-focusing. Therefore other mechanisms are required to understand such long-range filamentation. Kasparian et al. [15] performed ray-tracing calculation for long-range filamentation of fs laser pulse without taking ionization effect. The calculation suggests that the long filament results from the moving focus of spatial slices of the laser pulse. However, the ray-tracing simulations can be improved by using a more accurate intensity distribution of the laser field and including other physical processes, such as the ionization effect and temporal dynamics, which can also significantly influence the process of filamentation. To understand the long-range filamentation, we have proposed a scheme combining a (2D + 1) extended nonlinear Schrödinger (NLS) equation simulation with the spatiotemporal ray tracing calculation.

To describe the free propagation of fs laser pulses in air, we first present simulations on the basis of the (2D + 1) NLS equation coupled with the evolution equation of electron density. The NLS equation governs a slowly envelop of laser electric field E in the frame moving with the group-velocity v_g ($t \longrightarrow t - z/v_g$). The coupled equations can be written as:

$$\frac{\partial E}{\partial z} = i\frac{1}{2k_0}\Delta_\perp E - i\frac{k''}{2}\frac{\partial^2 E}{\partial t^2} + ik_0 n_2|E|^2 E - ik_0\frac{n_e}{2n_c}E - \frac{\beta^{(K)}}{2}|E|^{2K-2}E, \tag{1}$$

$$\frac{\partial n_e}{\partial t} = \frac{\beta^{(K)}}{K\hbar\omega_0}|E|^{2K}\left(1 - \frac{n_e}{n_{\mathrm{at}}}\right). \tag{2}$$

Here, $k_0 = 2\pi/\lambda_0$ ($\lambda_0 = 800$ nm) is the central wave number. The coordinate of Eq. (1) is cylindrically symmetric and the Laplacian operator $\Delta_\perp = \frac{\partial^2}{\partial r^2} + \frac{1}{r}\frac{\partial}{\partial r}$ denotes the beam transverse diffraction. Group-velocity dispersion is also included with coefficient $k'' = 0.2$ fs^2/cm. The remaining terms represents the Kerr self-focusing with coefficient $n_2 = 3.2 \times 10^{-19}$ cm^2/W, electron defocusing and multiphoton absorption with coefficient of $\beta^{(K)} = 3.1 \times 10^{-98}$ cm^{13}/W^7 for the number of photons $K = 8$. The electron in Eq. (2) is generated by multiphoton ionization of air. The critical plasma density and the neutral atoms density are $n_c = 1.7 \times 10^{21}$ cm^{-3} and $n_{\mathrm{at}} = 5.4 \times 10^{18}$ cm^{-3}, respectively.

Simulation was performed for a laser pulse with energy of 10 mJ, a peak power $P_{\mathrm{in}} = 27$ GW, a transverse waist (FWHM) $w = \sqrt{2\ln 2}w_0 = 10$ mm and a temporal duration (FWHM) $\tau = \sqrt{2\ln 2}\tau_0 = 350$ fs with negative chirp $c = -5.75$.

Figure 1 shows the distributions of energy fluence (a), peak intensity (b), and peak electron density (c) for the laser pulse propagating in air. A stable filament is formed and extends more than 100 m. During this process, the peak intensity of the filament reaches 8.1×10^{13} W/cm^2. The effective ionization is only observed at few short distances and the maximum of electron density is 4.9×10^{16} cm^{-3}.

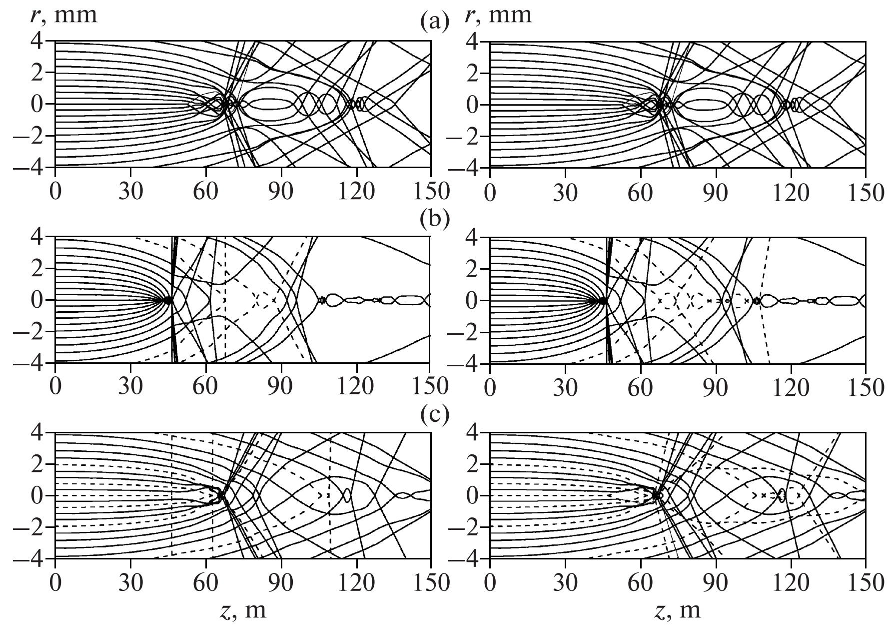

Fig. 2. The evolution of light rays for the time slice t = (a) −174, (b) 0, and (c) 174 fs when both the effects of Kerr nonlinearity and electron are considered (left) and only the Kerr nonlinearity is included (right).

In the ray-tracing calculations, the propagation of the laser pulse is considered as a bunch of light rays. The trajectory of each ray can be described by:

$$\frac{d^2r}{dz^2} = \nabla\eta, \tag{3}$$

where r is the position of the light rays and z is the propagation distance. The refractive index of air η is given by:

$$\eta = n_0 + n_2 I - \frac{n_e}{2n_c}, \tag{4}$$

where the n_0 is linear part, whose value is constant, and the nonlinear parts n_2I and $n_e/2n_c$ are induced by Kerr effect and ionization, respectively. To obtain the precise evolution of light rays, the values of intensity $I(r, t, z)$ and electron density $n_e(r, t, z)$ in Eq. (4) are taken from the numerical solution of NLS equation.

Figure 2 shows the trajectory of light rays for the time slice $t = -174$ (a), 0 (b), and 174 fs (c) in refractive index field $\eta = n_0 + n_2I - \frac{n_e}{2n_c}$ (left) and $\eta = n_0 + n_2I$ (right).

First, we investigate the trajectory of light rays when both the effects of Kerr nonlinearity and ionization are considered $\left(\eta = n_0 + n_2I - \frac{n_e}{2n_c}\right)$, as shown in Fig. 2 (left). For the different time slices, the common feature of light rays is that the rays from different start positions arrived to the beam axis at different propagation distance. And the focusing distance of rays essentially increases with their initial distance from beam axis, similar to the results in [15]. The central rays with higher intensity focus earlier than the rays in the fringe. Thus, it can be concluded the effect of moving focus can also be induced by the spatial distribution of laser intensity. During this process, the background energy replenishes the filament core over propagation distance. The mechanism of this kind of moving focus is described in [15]. From Fig. 2 (left) we can see that after the crossing with beam axis, some rays escape the beam but some rays can be trapped by the gradient of refractive index and return to the filament core again. The trajectory of rays is dependent to the incident angle on the beam axis and refractive index distribution. Comparing the trajectories of light rays with and without taking account of ionization effect $\left(\frac{n_e}{2n_c}\right)$, as shown in Fig. 2 (left) and Fig. 2 (right), we can see they are almost same except few rays which are drawn in dash line in Fig. 2. At some propagation distance the ionization effect can be able to change the direction of rays when the rays approach to the beam axis. However, the electrons are generated at a few short distances and only influence the laser field very close to the filament core.

Figure 3 shows the trajectory of light rays with the initial position $r_0 = 1$ (a), 2 (b), and 4 mm (c) for different time slices. For clarity, the figure only displays light rays from nine time slices. It can be seen that for the same start position, the rays of different time slices also approach to the beam axis at different distances.

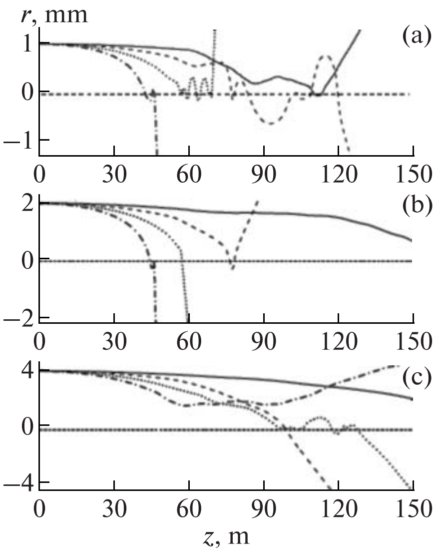

Fig. 3. The evolution of light rays with initial position $r_0 =$ (a) 1, (b) 2, and (c) 4 mm for the time slices $t = -278$ fs (solid line), -209 (dashed line), -139 (dotted line), and 0 fs (dash dot line).

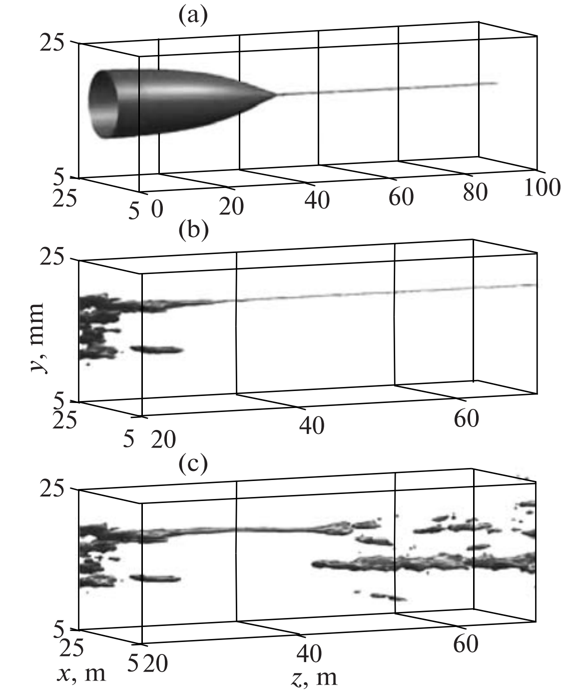

Fig. 4. The energy fluence distribution in unperturbed air (a). Energy fluence distribution in weak turbulent air with the structure constant $C_n^2 = 2.0 \times 10^{-17}$ m$^{-2/3}$ (b) and in moderate turbulent air with the structure constant $C_n^2 = 2.75 \times 10^{-16}$ m$^{-2/3}$ (c).

The rays from more intense time slice focus on the earlier propagation distance. These results are in good agreement with the model of moving focus proposed by Brodeur et al. [2]. Thus, we can see the spatiotemporal moving focus induced by the initial profile of the laser pulse is the dominating process for the formation of long filament.

Our calculations combining the NLS equation with the ray-tracing method show that the long filament is basically formed due to the moving focus induced by the initial distribution of laser intensity in spatial and temporal domain. The Kerr self-focusing is the dominated process during filamentation of the free propagated laser pulse. The self-guided mechanism due to dynamic balance between Kerr self-focusing and ionization defocusing may take place for filamentation of prefocused laser pulse in air or filamentation in solid and liquid media, where the electron density is much higher.

3. WIDENING OF LONG-RANGE FEMTOSECOND LASER FILAMENTS IN TURBULENT AIR

The influence of air turbulence on the long-range filamentation of fs laser pulses has been numerically investigated. Simulations are performed for different parameters of air turbulence and laser pulses. The results indicate that the diameter of filaments formed by free propagated fs laser pulses can be widened up to mm level by enough strong air turbulence. However, the widening effect can be suppressed if the propagating distance before the on-set position of filamentation becomes shorter. The reduction of non-linear focus length can be realized by pre-focusing of the laser pulse.

In our simulation, a negative chirped pulse with 270 fs duration is used to generate long range filament. The initial beam waist is 10 mm and the pulse energy is 10 mJ. The laser pulse has Gaussian shape in spatial and temporal domains. The pulse evolution of envelope during propagation is described by traditional NLS equation. The effects of the air turbulence on the laser propagation are usually simulated using thin phase screens which perturb the phase of a propagating wavefront [15]. The chain of phase screens, located along the propagation direction, reproduces adequately the properties of a continuous medium. The laser pulse will propagate freely between the two neighboring phase screens. To describe a wide range of refractive-index fluctuation we use the von Kármán model spectrum [12]. Figure 4a shows the isosurface of energy fluence of laser filament in unperturbed air. The energy fluence is normalized by the maximum in transverse plane for every propagation distance. From Fig. 4a, we can see the beam smoothly self-focused and a thin filament formed at the distance of 45 m. Figures 4b and 4c show the energy fluence distribution in weak ($C_n^2 = 2.0 \times 10^{-17}$ m$^{-2/3}$) and moderate ($C_n^2 = 2.75 \times 10^{-16}$ m$^{-2/3}$) turbulent atmosphere, respectively.

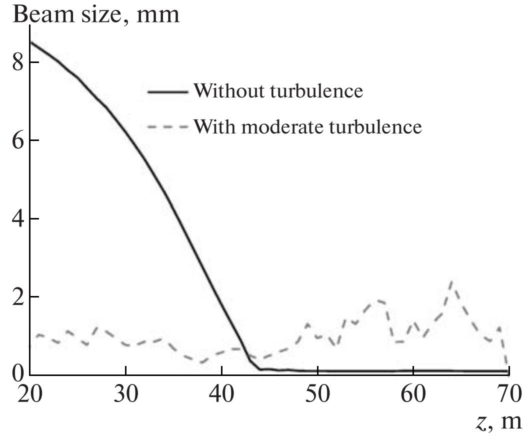

Fig. 5. The full-width-half-maximum of the beam size in unperturbed air (solid line) and in moderate turbulent air (dashed line). The structure constant of the turbulence air $C_n^2 = 2.75 \times 10^{-16}\ \mathrm{m}^{-2/3}$ and the inner scale is 1.0 mm.

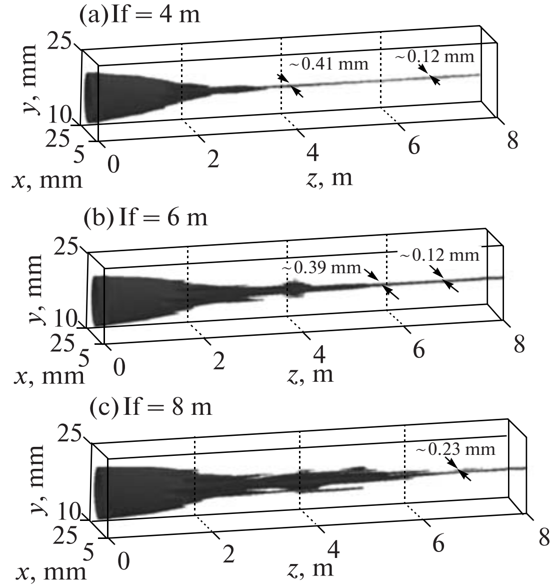

Fig. 6. The energy fluence distribution of the prefocused laser pulse propagating through turbulent atmosphere. The focal lengths of the convex lenses are (a) 4, (b) 6, and (c) 8 m. The structure constant of the turbulence air C_n^2 is $2.75 \times 10^{-16}\ \mathrm{m}^{-2/3}$ and the inner scale *lm* is 1.0 mm.

The inner scale, *lm*, is 1 mm. The beam profile is disturbed in the weak turbulent air (Fig. 2b) compared with that without turbulence in Fig. 2a. However, the energy still fuses into one thin filament in Fig. 4b. In Fig. 4c, the beam is randomly nucleated, forming a bath of spiky filaments over shorter distances (<30 m) in moderate turbulence. The center of the beam wanders before the beam collapsing [14, 16] and the energy fuses into one filament with widened diameter. We can see many small random local intensity peaks presented after the propagation distance of 70 m. These peaks are formed due to the random dynamics of laser field and disappear quickly. Only the continued and long channel is optical filament, whose length is much longer than the natural diffraction (Rayleigh) length for the beam waist of this optical filament. The beam diameter sustains about 1–2 mm in long propagation distance (Fig. 5, dashed line). The inner scale of moderate turbulence in our simulation is 1 mm. This is smaller than the transverse size of filament and much smaller than the background energy reservoir, which is extended to cm distance from the filament center for such long filament. As a result, the air turbulence causes phase perturbations on the energy background and this perturbation can be accumulated with propagation distance. The distortion of wave front can partly break the process of energy replenishment from background reservoir to the filament core [17]. Thus, this effect can lead the widening of filament size on large distance propagation and decrease of the filament intensity to 10^{12} W/cm^2 which is around the ionization threshold of air.

Figure 6 shows the energy fluence distribution when a laser pulse with 10 mJ energy is prefocused by the lenses of focal length 4 (a), 6 (b), and 8 m (c). Although the turbulent air is the same as the free propagation (Fig. 4b), we can see from Fig. 6 that the transverse widths of the filaments are very small for all focal conditions, which agrees well with both numerical and experimental results [18, 19]. Earlier experiment [20] shows that for filamentation of prefocused laser pulses, the size of energy background is about 1mm, which is comparable to the inner scale of air turbulence. In this case, the energy background is weakly influenced by the turbulent air. The energy exchanges between the filament and background forming a thin filament, as that in unperturbed air. The influence of the air turbulence reduces with the decreasing of the on-set position of filamentation. This is consistent with the experiment of [21] which reported that a thin filament can be generated by a prefocusing beam even under strong turbulent air.

4. FILAMENTATION OF INTERACTING FEMTOSECOND LASER PULSES IN AIR

The filamentation of two co-propagated fs laser pulses in air has been studied by numerical simulation. Depending on the different initial separation distances, relative phase shift and crossing angles, simulations show attraction, fusion, repulsion and collision of the two pulses. A long and stable plasma channel can be formed by two in-phase pulses with small separation distance and cross angle. The coupling of two laser pulses becomes weak when the separation distance or cross angle are large. In this case, the filamentation of each pulse developed independently.

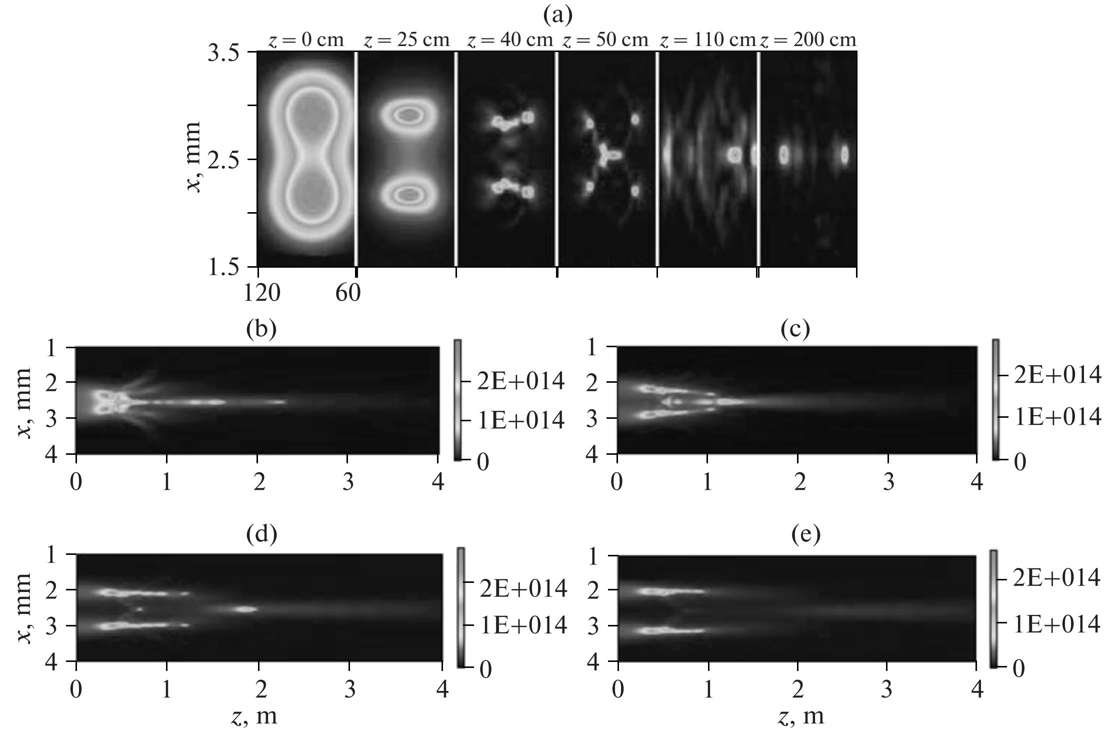

Fig. 7. The spatiotemporal intensity distribution of two parallel in-phase interacting Gaussian pulses with the initial separation distance $\Delta_0 = 0.78$ mm (a). The energy fluence distributions at different initial separation distances $\Delta_0 = 0.62$ (b), 0.78 (c), 0.94 (d), and 1.09 mm (e).

In our simulation, two identical Gaussian pulses with 40 fs duration, 1 mJ energy, and 0.59 mm waist are used. Figure 7a illustrates the spatiotemporal intensity distribution of in-phase parallel Gaussian pulses with initial separation distances, $\Delta_0 = 0.78$ mm. It is shown that two pulses collapse at $z = 30$ cm and temporally break into two subpulses at $z = 50$ cm, respectively. The filaments then defocus by the induced plasma and more energy disperses outside. Because the two pulses interfere constructively, the intensity in the overlapping region becomes larger which leads to a larger refractive index in the center due to the Kerr effect. Thus the background energy is attracted towards the center, resulting in a new filament at $z = 120$ cm.

Figures 7b–7e show the interaction of two in-phase parallel Gaussian pulses with different initial separation distances, $\Delta_0 = 0.62$, 0.78, 0.94, and 1.09 mm. The initial separation distance plays an important role in the interaction of the pulses. If the initial separation distance is comparable to the waist of each pulse (Fig. 7b), the merging process starts earlier. The merging of filaments prolongs the filament's length and the plasma channel's length by comparison with filamentation of a single beam. When the separation distance is much larger than the initial transverse waist of each Gaussian pulses, the filamentation of each pulse developed independently (Fig. 7e).

For the out-of-phase case, two pulses repel each other and disperse quickly if the initial separation distance is small. When the separation distance is large, the filamentation of pulses developed independently. In addition, our simulation also indicates that for large crossing angle, two pulses meet, go through each other and then disperse quickly. Our simulation results can be helpful for understanding the influence of the initial intensity and phase modulation of laser pulses on the filamentation.

5. CONCLUSIONS

The mechanism of long-range filamentation of fs laser pulses in air, the influence of the air turbulence on the filamentation, and the interaction of two intense fs pulses and the resulting filaments are investigated numerically. The simulations combining the NLS simulations with the ray-tracing calculations show that a long filament is basically formed due to the moving focus induced by the initial distribution of the laser intensity in the spatial and temporal domains. Air turbulence causes random fluctuations of refractive index of the atmosphere. Widening filament with a length of hundred meters is induced by the perturbation of air turbulence. The attraction, fusion, repulsion and collision of the two pulses can occur depending on the initial separation distances, relative phase shift and crossing angles.

ACKNOWLEDGMENTS

This work is supported by the National Natural Science Foundation of China (Grant nos. 60621063, 10634020, and 10734130), the National Basic Research Program of China (973 Program) (Grant no. 2007CB815101).

REFERENCES

1. A. Braun, G. Korn, X. Liu, D. Du, J. Squier, and G. Mourou, Opt. Lett. **20**, 73 (1995).
2. A. Brodeur, C. Y. Chien, F. A. Ilkov, S. L. Chin, O. G. Kosareva, and V. P. Kandidov, Opt. Lett. **22**, 304 (1997).
3. J. H. Marburger and W. G. Wagner, IEEE J. Quantum Electron. **QE-3**, 415 (1967).
4. V. N. Lugovoi and A. M. Prokhorov, JETP Lett. **7**, 117 (1968).
5. M. M. Loy and Y. R. Shen, Phys. Rev. Lett. **22**, 994 (1969).
6. M. Mlejnek, E. M. Wright, and J. V. Moloney, IEEE J. Quantum Electron. **35**, 1771 (1999).
7. M. Mlejnek, E. M. Wright, and J. V. Moloney, Opt. Lett. **23**, 382 (1998)
8. S. Tzortzakis, L. Bergé, A. Couairon, M. Franco, B. Prade, and A. Mysyrowicz, Phys. Rev. Lett. **86**, 5470 (2001).
9. G. Méchain, A. Couairon, M. Franco, B. Prade, and A. Mysyrowicz, Phys. Rev. Lett. **93**, 035003 (2004).
10. Zuo-Qiang Hao, Jie Zhang, Xin Lu, Ting-Ting Xi, Yu-Tong Li, Xiao-Hui Yuan, Zhi-Yuan Zheng, Zhao-Hua Wang, Wei-Jun Ling, and Zhi-Yi Wei, Opt. Express **14**, 773 (2006).
11. M. Rodriguez, R. Bourayou, G. Méjean, J. Kasparian, J. Yu, E. Salmon, A. Scholz, B. Stecklum, J. Eilsöffel, U. Laux, A. P. Hatzes, R. Sauerbrey, L. Wöste, and J. P. Wolf, Phys. Rev. E **69**, 036607 (2004).
12. G. Méchain, A. Couairon, Y. -B. André, C. D'Amico, M. Franco, B. Prade, S. Tzortzakis, A. Mysyrowicz, and R. Sauerbrey, Appl. Phys. B **79**, 379 (2004).
13. F. Théberge, Q. Luo, W. Liu, S. A. Hosseini, M. Sharifi, and S. L. Chin, Appl. Phys. Lett. **87**, 081108 (2005).
14. G. Méchain, C. D'Amico, Y. -B. André, S. Tzortzakis, M. Franco, B. Prade, A. Mysyrowicz, A. Couairon, E. Salmon, and R. Sauerbrey, Opt. Comm, **247**, 171 (2005).
15. J. Kasparian, J. Sole, M. Richard, and J.-P. Wolf, Appl. Phys. B **79**, 947 (2004).
16. V. P. Kandidov, O. G. Kosareva, I. S. Golubstov, W. Liu, A. Becker, N. Akozbek, C. M. Bowden, and S. L. Chin, Appl. Phys. B **77**, 149 (2003).
17. Z. Q. Hao, J. Zhang, Z. Zhang, X. H. Yuan, Z. Y. Zheng, X. Lu, Z. H.Wang, J. Y. Zhong, and Y. Q. Liu, Phys. Rev. E **74**, 066402 (2006).
18. T. T. Xi, X. Lu, and J. Zhang, Phys. Rev. Lett. **96**, 025003 (2006).
19. A. Couairon, S. Tzortzakis, L. Berg'e, M. Franco, B. Prade, and A. Mysyrowicz, J. Opt. Soc. Am. B **19**, 1117 (2002).
20. E. M. Johanson and D. T. Gavel, Proc. SPIE **2200**, 372 (1994).
21. J. Kasparian and J.-P. Wolf, Opt. Express **16**, 466 (2007).